THE JOURNAL OF PHYSICAL CHEMISTRY Letters

Letter

pubs.acs.org/JPCL

Jahn–Teller Effect on Framework Flexibility of Hybrid Organic–Inorganic Perovskites

Di Gui,[†] Lijun Ji,[†] Azeem Muhammad,[†] Wei Li,*[,†] Weizhao Cai,*[,‡] Yanchun Li,[§] Xiaodong Li,[§] Xiang Wu,*[,∥] and Peixiang Lu*[,†,⊥]

[†]School of Physics and Wuhan National Laboratory for Optoelectronics, Huazhong University of Science and Technology, Wuhan 430074, China

[‡]Department of Physics and Astronomy, University of Utah, Salt Lake City, Utah 84112, United States

[§]Beijing Synchrotron Radiation Facility, Institute of High Energy Physics, Chinese Academy of Sciences, Beijing 100049, China

[∥]State Key Laboratory of Geological Processes and Mineral Resources, China University of Geosciences, Wuhan 430074, China

[⊥]Laboratory for Optical Information Technology, Wuhan Institute of Technology, Wuhan 430205, China

Supporting Information

ABSTRACT: Here we study the Jahn–Teller (JT) effect on framework flexibility of two analogous hybrid organic–inorganic perovskites, $[C(NH_2)_3][Zn(HCOO)_3]$ (1-Zn) and $[C(NH_2)_3][Cu(HCOO)_3]$ (2-Cu). Single-crystal nanoindentation measurements show that the elastic moduli and hardnesses of 1-Zn are up to ∼52.0% and ∼25.0% greater than those of the JT active 2-Cu. Temperature-dependent X-ray diffraction measurements indicate that the thermal expansion along the *b*-axis is switched from negative to positive by replacing Zn^{2+} with Cu^{2+} on the B-site. These stark distinctions in framework flexibility are primarily attributed to the ∼10.0% elongation of Cu–O bonds induced by the JT effect and associated alterations in octahedral tilting and hydrogen-bonding. Our results demonstrate the prominence of the JT effect in the emerging hybrid perovskites and highlight the possibilities of tuning materials' properties using orbital order.

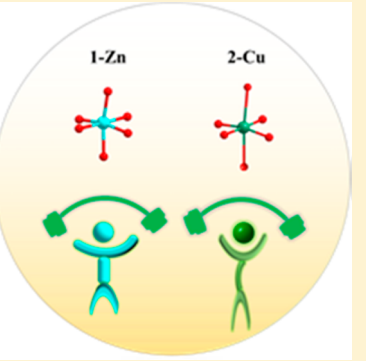

The JT effect arises from the fact that degenerate electronic states can undergo a lowered energy of their ground state by lifting this degeneracy via a geometrical distortion.[1] This orbital order with a quadrupolar nature has far-reaching consequences in modern chemistry and physics of perovskite materials because the emergence of JT active transition metal ions (e.g., Cu^{2+}, Cr^{2+}) on the B-site significantly complicates the electronic nature of the structure.[2] Such JT coupling triggers low-symmetry MX_6 octahedral distortions which are responsible for many intriguing properties in perovskite oxides. For example, the discovery of high-temperature superconductivity in cuprates is largely related to the electron pairing via the JT polaron formation.[3] Likewise, the origin of colossal magnetoresistance in manganites involves the JT distortion-induced lattice-polaronic effects.[4]

Recently, the significance of JT effect has been increasingly noted by researchers in the emerging field of hybrid organic–inorganic perovskites (HOIPs).[5−10] Compared with compact conventional ABO_3 perovskites, the presence of organic components in HOIPs enables the JT distortion to influence the perovskite structure and corresponding physical properties via hydrogen bonding and other dispersion forces.[11−13] For example, in $[Gua][Cu(HCOO)_3]$ (Gua = $C(NH_2)_3^+$), the coupling of the JT effect and the A-site organic Gua cation via hydrogen bonding induces the occurrence of a new type of hybrid improper ferroelectricity which is not possible in conventional perovskites.[5]

More interestingly, further theoretical studies about another JT active analogue, $[Gua][Cr(HCOO)_3]$, reveal the hybridization of the JT distortion of Cr^{2+}, and the rotational modes of the Gua cation can also induce such improper ferroelectric ordering.[8] A very recent experimental work echoes the aforementioned significance of the JT effect in creating new functionalities by showing the facile control from an orbital order–disorder to a multipolar reorientation transition through simply varying the metal composition of $[Gua][Cu_xCd_{1-x}(HCOO)_3]$.[10] Motivated by these unprecedented discoveries, exploiting the JT effect in HOIPs is particularly meaningful and could provide new avenues for creating novel functionalities that traditional JT active perovskites cannot endow.[14]

Here we study the JT effect on the framework rigidity and thermal expansion of $[Gua][Zn(HCOO)_3]$ (1-Zn) by comparison with the JT active analogue $[Gua][Cu(HCOO)_3]$ (2-Cu). Both 1-Zn and 2-Cu crystallize in the orthorhombic system with comparable lattice parameters (*Pnna*, a = 8.3493(3) Å, b = 8.9089(4) Å, and c = 11.7276(5) Å for 1-Zn; $Pna2_1$, a = 8.5212(3) Å, b = 9.0321(3) Å, and c = 11.3497(4) Å for 2-

Received: December 5, 2017
Accepted: January 23, 2018
Published: January 23, 2018

DOI: 10.1021/acs.jpclett.7b03229
J. Phys. Chem. Lett. XXXX, XXX, XXX–XXX

Cu).[15] In their perovskite-like structures, the A-, B-, and X-sites are Gua, Cu^{2+}/Zn^{2+}, and $HCOO^-$, respectively (Figure 1a,b).

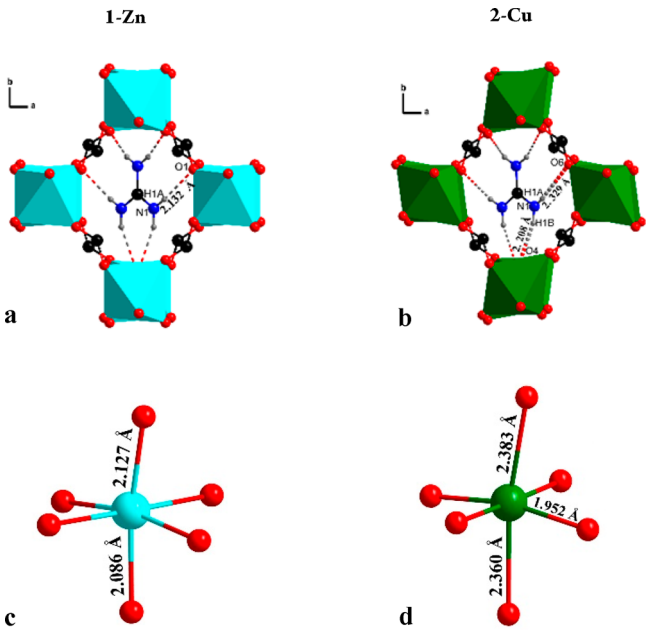

Figure 1. Framework structures of [Gua][$Zn(HCOO)_3$] (1-Zn) (a) and [Gua][$Cu(HCOO)_3$] (2-Cu) (b); the coordination environments of Zn^{2+} and Cu^{2+} ions in 1-Zn (c) and 2-Cu (d). Color scheme: Zn^{2+}, turquoise; Cu^{2+}, green; N, blue; O, red; C, black; H, gray. The N−H···O bonds are presented as dashed lines, and the two thicker dashed lines in panel b highlight the elongated H···O bonds induced by the JT effect in 2-Cu.

In addition, eEach $[C(NH_2)_3^+]$ cation forms six N−H···O hydrogen bonds with the pseudocubic framework unit in both compounds. Though the atomic radii of Zn^{2+} and Cu^{2+} are almost identical (0.74 Å vs 0.73 Å), their coordination bond distances are significantly different. In 1-Zn, the ZnO_6 octahedra exhibit a trivially distorted coordination geometry with Zn−O bond lengths ranging from 2.086 to 2.127 Å. However, two Cu−O bonds are significantly elongated to 2.360 and 2.383 Å, and the other four are compressed to 1.852−2.000 Å in the CuO_6 octahedra of 2-Cu (Figure 1c,d). Although the CuO_6 octahedron deforms considerably, the magnitudes of O−Cu−O angles (82.26−105.87° and 168.34−179.25°) are comparable to the corresponding O−Zn−O angles (82.27−105.53° and 167.2−178.85°). Interestingly, the adjacent JT axes of CuO_6 octahedra within the *ab*-plane are arranged alternatively orthogonal along [110] and [$\bar{1}$10], leading to an anisotropic packing fashion compared with that in 1-Zn.

We first examine the JT effect on elastic modulus (*E*) and hardness (*H*) properties. Nanoindentation measurements were performed on selected 1-Zn and 2-Cu single crystals using a three-sided pyramidal Berkovich tip in the quasi-static mode,[16−19] where the indenter was along the orientations of the principal axes [normal to ($\bar{1}$10), (110), and ($\bar{1}$10)], face diagonals [normal to ($\bar{1}$11) and (1$\bar{1}$1)], and body diagonal [normal to (011)] of the pseudocubic perovskite unit cell (Figures S1 and S2), respectively. Representative load−indentation depth (*P*−*h*) curves obtained on relevant crystal faces of both HOIPs are displayed in Figure 2a (full data are shown in Figures S3 and S4). Clearly, faces of 2-Cu crystals were indented to much greater depths compared to those of 1-Zn crystals at the same load, indicating its less framework rigidity.[20,21] The average values of the *E* and *H* normal to relevant crystal faces of 1-Zn and 2-Cu are shown in Figure 2b,c and Table S1.[22] Strikingly, the *E* values of 1-Zn are up to ∼38.0%, 52.0%, and 49.0% greater than those of 2-Cu along the axial, face-diagonal, and body-diagonal directions, respectively. The *H* values show a similar trend, though the discrepancies are reduced to ∼25.0%, 13.0%, and 21.0%, respectively.

To understand the origin of the marked difference in *E* and *H* between these two HOIPs, we examine their underlying molecular structures. As the O−Zn−O and O−Cu−O angles show only less than 1.0% difference, the bond angles do not lead to any significant influences in framework robustness.[15] In this regard, the substantial difference in mechanical strengths between 1-Zn and 2-Cu primarily arises from the 10.0% elongation of Cu−O bond lengths due to the strong JT distortions. As expected, the stretched Cu−O bonds can be more easily deformed under indentation stress compared with the nondistorted Zn−O bonds; thus, 2-Cu is significantly more compliant than 1-Zn. Interestingly, the least difference in *E* between 1-Zn and 2-Cu occurs from the axial direction, while their face- and body-diagonal directions show larger modulus differences. As seen in Figures S1 and S2, half and all JT axes in the pseudo cubic unit cell of 2-Cu are deformed when being indented axially and diagonally, respectively. The former indentation situation involves less compliant CuO_6 octahedra than the later, hence resulting in lower rigidity contrasts along axial orientations than diagonal directions. In terms of hardness properties, the lower resistance of 2-Cu toward plastic deformation also mainly arises from the drastic elongation of the Cu−O bonds due to the JT distortion. The vulnerable Cu−O bonds are more sensitive to external stress, which could generate more ruptures and facilitate the formation of more dislocations and slippages, hence giving rise to much lower *H* values compared with the zinc counterpart.[23]

Moreover, we investigate the thermally induced framework flexibility of 1-Zn and 2-Cu in the range of 120−300 K via temperature-dependent single-crystal X-ray diffraction (SCXRD). As shown in Table S2, no phase transitions are observed in both HOIPs in the measured temperature range. Upon heating, both 1-Zn and 2-Cu expand linearly along the *a* and *c* axes with thermal expansion coefficients $\alpha_{a(1\text{-}Zn)} = 39.8(3)$ and $\alpha_{c(1\text{-}Zn)} = 26.6(5)$ MK^{-1}, and $\alpha_{a(2\text{-}Cu)} = 51.8(5)$ and $\alpha_{c(2\text{-}Cu)=}$ $25.7(5)$ MK^{-1}, respectively (Figures S5).[24−26] Strikingly, 1-Zn exhibits negative thermal expansion (NTE) along the *b*-axis with $\alpha_{b(1\text{-}Zn)} = -5.2(5)$ MK^{-1}, while 2-Cu shows positive thermal expansion (PTE) along corresponding direction $\alpha_{b(2\text{-}Cu)} = 3.2(7)$ MK^{-1} (Figure 3a). Such an interesting positive-to-negative switch is primarily attributed to the distinct hydrogen-bonding modes in these two HOIPs. To elucidate the NTE mechanism in 1-Zn, we decompose the six hydrogen bonds within a pseudocubic unit cell along three orthogonal axes. As seen in Table S3, the total projections of hydrogen-bonding (N−H···O distance) along the *b*-axis is ∼50% larger than that along *a*,[27] which consequently leads to significantly higher constraints of the pseudocubic unit cell along *b*- than *a*-axis upon thermal perturbation. In this regard, the *a*-axis expands so rapidly that the *b*-axis has to shrink upon heating as illustrated using the "hinge-strut" model in Figure 3b.[28] However, the situation in 2-Cu is different because of the lattice distortion induced by the JT effect. Though the total projections of hydrogen-bonding along *a*- and *b*-axis in 2-Cu are reminiscent of those in 1-Zn, the hydrogen-bonding angle

DOI: 10.1021/acs.jpclett.7b03229
J. Phys. Chem. Lett. XXXX, XXX, XXX−XXX

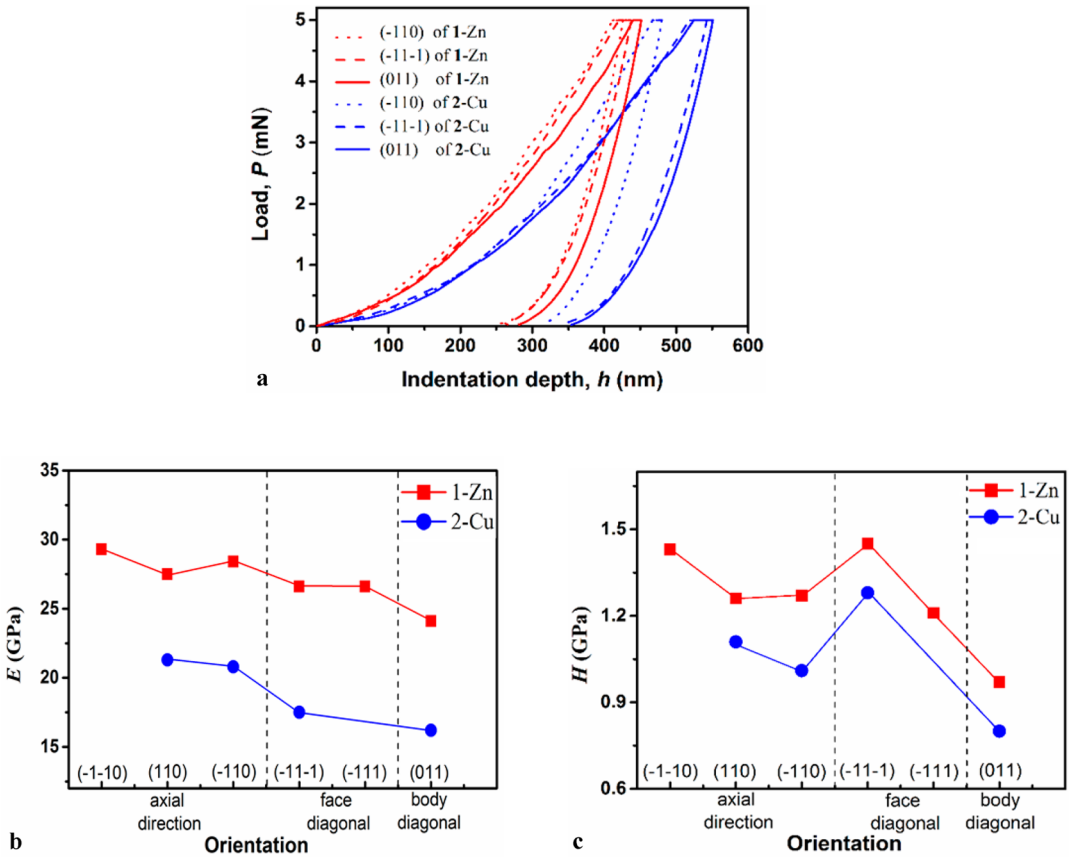

Figure 2. (a) Representative load−indentation depth (P−h) curves, obtained normal to the axial, face-diagonal, and body-diagonal direction oriented facets of 1-Zn and 2-Cu crystals; extracted experimental data of (b) E and (c) H. The error bars are smaller than experimental data points (the lines drawn between data points give a guide to the eye).

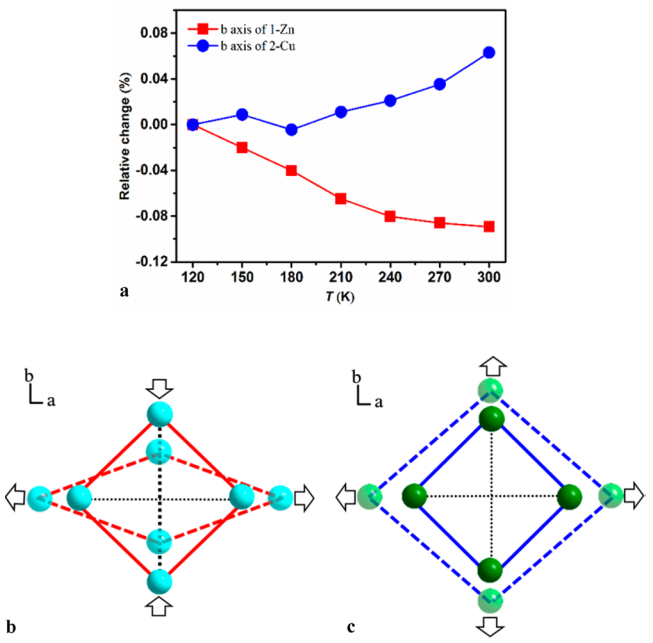

Figure 3. Thermal expansion behavior of frameworks 1-Zn and 2-Cu. (a) Relative changes of b-axis lengths of 1-Zn and 2-Cu as a function of temperature (T); (b, c) "hinge-strut" models of 1-Zn and 2-Cu at low (solid lines) and high temperature (dashed lines), where the black dotted lines represent the summed hydrogen-bonding along the a- and b-axis and the thickness of the lines indicates their strengths.

changes dramatically. As seen in Tables S4, the bond angles of N1−H1A···O6 and N1−H1B···O4 in 2-Cu are ∼9° and ∼2° larger than the corresponding N1−H1A···O1 angle in 1-Zn, which lead to ∼0.20 and ∼0.08 Å longer H1A···O6 and H1B···O4 bond lengths. These stretched H-bonds significantly weaken the linking strengths between the Gua and framework along the b-axis in 2-Cu, thus giving rise to large enough thermal expansivity which cannot be compensated by the a-axis expansion upon heating. Such a cooperative process, coupled with octahedral tilting, lead to an opposite "hinge-strut" motion (Figure 3c) compared with the scenario 1-Zn; hence, PTE occurs along the b-axis in 2-Cu. Additional structural data are detailed in Figures S6 and S7 and Table S5.

As the hydrogen-bonding constraints in 2-Cu are weaker than those in 1-Zn, its framework vibration is expected to be larger than that of 1-Zn.[22] This is confirmed by the equivalent isotropic atomic displacement parameters (U_{iso}) of the B-site metal ions extracted from temperature-dependent SCXRD, where the U_{iso} of Cu atoms are ∼50% larger than those of Zn atoms in the whole measured temperature range (Figure 4), indicating the average positions of Cu atoms in 2-Cu are less localized upon heating.

We also performed high-pressure powder X-ray diffraction measurements to compare the hydrostatic behavior between 1-Zn and 2-Cu (Figures S8−S10 and Table S6). Our results reveal the 1-Zn and 2-Cu exhibit pressure-induced phase transitions at about 1.82−2.87 and 0.66−0.82 GPa, respectively, demonstrating 2-Cu is less robust than 1-Zn under hydrostatic conditions (Figure S8). The unit cell volume (V) versus

DOI: 10.1021/acs.jpclett.7b03229
J. Phys. Chem. Lett. XXXX, XXX, XXX−XXX

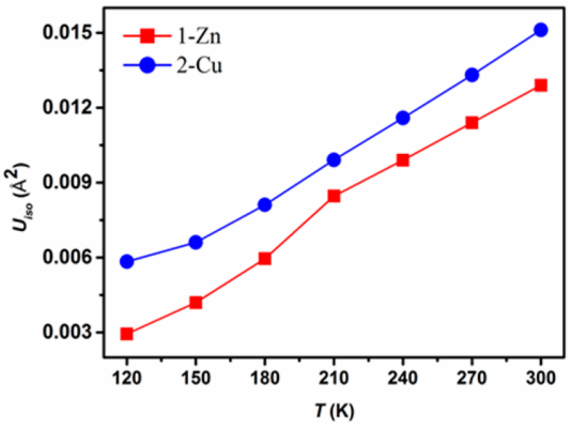

Figure 4. Equivalent isotropic atomic displacement parameters (U_{iso}) for zinc atoms in framework 1-Zn and copper atoms in 2-Cu as a function of temperature (T).

pressure (P) data prior to phase transitions (0−1.82 GPa for 1-Zn, 0−0.66 GPa for 2-Cu) were fit with the second-order Birch−Murnaghan equations of state using the PASCal software,[24] and the isothermal bulk moduli (B) of 2-Cu is 25.6(29) GPa, which is smaller than the 30.3(28) GPa of 1-Zn, further indicating the higher framework flexibility of 2-Cu over 1-Zn.

In summary, we have investigated the JT effect on the framework flexibility of two analogous hybrid perovskites 1-Zn and 2-Cu using combined nanoindentation and diffraction techniques. Our results show that these two compounds exhibit significantly different elastic moduli, hardnesses, thermal expansion, and high-pressure behavior which are primarily caused by their distinct M−O (M = Cu, Zn) bond lengths induced by the strong JT distortion. Our present work demonstrates the prominence of JT effect on physical properties of HOIPs and also provides the principles of controlling materials' properties using another type of degree of freedom, namely orbital order.[10]

■ ASSOCIATED CONTENT

Supporting Information

The Supporting Information is available free of charge on the ACS Publications website at DOI: 10.1021/acs.jpclett.7b03229.

CIF files (ZIP)

Experimental details and supplementary figures, graphs, and tables (PDF)

■ AUTHOR INFORMATION

Corresponding Authors

*E-mail: wl276@hust.edu.cn.

*E-mail: wzhcai@gmail.com.

*E-mail: wuxiang@cug.edu.cn.

*E-mail: lupeixiang@hust.edu.cn.

ORCID

Wei Li: 0000-0002-5277-6850

Weizhao Cai: 0000-0001-7805-2108

Notes

The authors declare no competing financial interest.

■ ACKNOWLEDGMENTS

D.G. and W.L. are grateful to Prof. Zheming Wang for single-crystal X-ray diffraction measurements. All authors acknowledge the funding support from the National Natural Science Foundation of China (Nos. 21571072, 11374114, 10974062).

■ REFERENCES

(1) Englman, R.; Dow, J. D. *The Jahn-Teller Effect in Molecules and Crystals*; Wiley Interscience: New York, 1972.

(2) Bersuker, I. B. *The Jahn-Teller Effect*; Cambridge University Press: Cambridge, 2006.

(3) Keller, H.; Bussmannholder, A.; Muller, K. A. Jahn-Teller Physics and High-T_c Supercond-uctivity. *Mater. Today* **2008**, *11*, 38−46.

(4) Millis, A. J.; Shraiman, B. I.; Mueller, R. Dynamic Jahn-Teller Effect and Colossal Magneto-resistance in $La_{1-x}Sr_xMnO_3$. *Phys. Rev. Lett.* **1996**, *77*, 175−178.

(5) Stroppa, A.; Jain, P.; Barone, P.; Marsman, M.; Perez-Mato, J. M.; Cheetham, A. K.; Kroto, H. W.; Picozzi, S. Electric Control of Magnetization and Interplay between Orbital Ordering and Ferroelec-tricity in a Multiferroic Metal-Organic Framework. *Angew. Chem.* **2011**, *123*, 5969−5972.

(6) Tian, Y.; Stroppa, A.; Chai, Y. S.; Barone, P.; Perez-Mato, M.; Picozzi, S.; Sun, Y. High-Temperature Ferroelectricity and Strong Magnetoelectric Effects in a Hybrid Organic-Inorganic Perovskite Framework. *Phys. Status Solidi RRL* **2015**, *9*, 62−67.

(7) Fan, F. R.; Wu, H.; Nabok, D.; Hu, S.; Ren, W.; Draxl, C.; Stroppa, A. Electric-Magneto-Optical Kerr Effect in a Hybrid Organic-Inorganic Perovskite. *J. Am. Chem. Soc.* **2017**, *139*, 12883−12886.

(8) Stroppa, A.; Barone, P.; Jain, P.; Perez-Mato, J. M.; Picozzi, S. Hybrid Improper Ferroele-ctricity in a Multiferroic and Magneto-electric Metal-Organic Framework. *Adv. Mater.* **2013**, *25*, 2284−2290.

(9) Wang, Z. X.; Jain, P.; Choi, K. Y.; Tol, J. V.; Cheetham, A. K.; Kroto, H. W.; Koo, H. J.; Zhou, H. D.; Hwang, J. M.; Choi, E. S.; et al. Dimethylammonium Copper Formate $[(CH_3)_2NH_2]$ $Cu(HCOO)_3$: A Metal-Organic Framework with Quasi-One-Dimensional Antiferro-magnetism and Magnetostriction. *Phys. Rev. B: Condens. Matter Mater. Phys.* **2013**, *87*, 22406.

(10) Evans, N. L.; Thygesen, P. M. M.; Boström, H. L. B.; Reynolds, E. M.; Collings, I. E.; Phillips, A. E.; Goodwin, A. L. Control of Multipolar and Orbital Order in Perovskite-Like $[C(NH_2)_3]$ $Cu_xCd_{1-x}(HCOO)_3$ Metal-Organic Frameworks. *J. Am. Chem. Soc.* **2016**, *138*, 9393−9396.

(11) Saparov, B.; Mitzi, D. B. Organic-Inorganic Perovskites: Structural Versatility for Functio-nal Materials Design. *Chem. Rev.* **2016**, *116*, 4558−4596.

(12) Li, W.; Wang, Z. M.; Deschler, F.; Gao, S.; Friend, R. H.; Cheetham, A. K. Chemically Diverse and Multifunctional Hybrid Organic-Inorganic Perovskites. *Nat. Rev. Mater.* **2017**, *2*, 16099−16117.

(13) Xu, W. J.; Du, Z. Y.; Zhang, W. X.; Chen, X. M. Structural Phase Transitions in Perovskite Compounds Based on Diatomic or Multiatomic Bridges. *CrystEngComm* **2016**, *18*, 7915−7928.

(14) Cheetham, A. K.; Rao, C. N. R. There's Room in the Middle. *Science* **2007**, *318*, 58−59.

(15) Hu, K. L.; Kurmoo, M.; Wang, Z. M.; Gao, S. Metal-Organic Perovskites: Synthesis, Structures, and Magnetic Properties of $[C(NH_2)_3][M^{II}(HCOO)_3]$ (M = Mn, Fe, Co, Ni, Cu, and Zn; $C(NH_2)_3$=Guanidinium). *Chem. - Eur. J.* **2009**, *15*, 12050−12064.

(16) Tan, J. C.; Cheetham, A. K. Mechanical Properties of Hybrid Inorganic-Organic Framework Materials: Establishing Fundamental Structure-Property Relationships. *Chem. Soc. Rev.* **2011**, *40*, 1059−1080.

(17) Ramamurty, U.; Jang, J. Nanoindentation for Probing the Mechanical Behavior of Molecular Crystals-a Review of the Technique and How to Use It. *CrystEngComm* **2014**, *16*, 12−23.

(18) Varughese, S.; Kiran, M. S. R. N.; Ramamurty, U.; Desiraju, G. R. Nanoindentation in Crystal Engineering: Quantifying Mechanical

DOI: 10.1021/acs.jpclett.7b03229
J. Phys. Chem. Lett. XXXX, XXX, XXX−XXX

297 Properties of Molecular Crystals. *Angew. Chem., Int. Ed.* **2013**, *52*,
298 2701−2712.
299 (19) Li, W.; Henke, S.; Cheetham, A. K. Research Update:
300 Mechanical Properties of Metal-Organic Frameworks-Influence of
301 Structure and Chemical Bonding. *APL Mater.* **2014**, *2*, 123902−
302 123911.
303 (20) Varughese, S.; Kiran, M. S. R. N.; Solanko, K. A.; Bond, A. D.;
304 Ramamurty, U.; Desiraju, G. R. Interaction Anisotropy and Shear
305 Instability of Aspirin Polymorphs Established by Nanoin-dentation.
306 *Chem. Sci.* **2011**, *2*, 2236−2242.
307 (21) Kiran, M. S. R. N.; Varughese, S.; Reddy, C. M.; Ramamurty, U.;
308 Desiraju, G. R. Mechanical Anisotropy in Crystalline Saccharin:
309 Nanoindentation Studies. *Cryst. Growth Des.* **2010**, *10*, 4650−4655.
310 (22) Li, W.; Thirumurugan, A.; Barton, P. T.; Lin, Z. S.; Henke, S.;
311 Yeung, H. H. M.; Wharmby, M. T.; Bithell, E. G.; Howard, C. J.;
312 Cheetham, A. K. Mechanical Tunability via Hydrogen Bonding in
313 Metal-Organic Frameworks with the Perovskite Architecture. *J. Am.*
314 *Chem. Soc.* **2014**, *136*, 7801−7804.
315 (23) Horie, Y.; Davison, L.; Thadani, N. *High-Pressure Shock*
316 *Compression of Solids VI: Old Paradigms and New Challenges*;
317 Springer-Verlag, Academic: New York, 2003, 291.
318 (24) Cliffe, M. J.; Goodwin, A. L. Pascal: A Principal Axis Strain
319 Calculator for Thermal Expansion and Compressibility Determination.
320 *J. Appl. Crystallogr.* **2012**, *45*, 1321−1329.
321 (25) Collings, I. E.; Hill, J. A.; Cairns, A. B.; Cooper, R. I.;
322 Thompson, A. L.; Parker, J. E.; Tang, C. C.; Goodwin, A. L.
323 Compositional Dependence of Anomalous Thermal Expansion in
324 Perovskite-Like ABX_3 Formates. *Dalton Trans.* **2016**, *45*, 4169−4178.
325 (26) Feng, G. Q.; Ma, J.; Gui, D.; Li, Z. H.; Li, W. Negative Thermal
326 Expansion Properties of Two Metal-Organic Perovskite Frameworks.
327 *Chin. J. Inorg. Chem.* **2017**, *33*, 932−938.
328 (27) Sun, S.; Henke, S.; Wharmby, M. T.; Yeung, H. H. M.; Li, W.;
329 Cheetham, A. K. Mechanical Properties of a Calcium Dietary
330 Supplement, Calcium Fumarate Trihydrate. *Inorg. Chem.* **2015**, *54*,
331 11186−11192.
332 (28) Ogborn, J. M.; Collings, I. E.; Moggach, S. A.; Thompson, A. L.;
333 Goodwin, A. L. Supra-molecular Mechanics in a Metal-Organic
334 Framework. *Chem. Sci.* **2012**, *3*, 3011−3017.

DOI: 10.1021/acs.jpclett.7b03229
J. Phys. Chem. Lett. XXXX, XXX, XXX−XXX